

# HX-POL – A Balloon-Borne Hard X-Ray Polarimeter

H. Krawczynski<sup>1</sup>, A. Garson III<sup>1</sup>, J. Martin<sup>1</sup>, Q. Li<sup>1</sup>, M. Beilicke<sup>1</sup>, P. Dowkontt<sup>1</sup>, K. Lee<sup>1</sup>, E. Wulf<sup>2</sup>, J. Kurfess<sup>3</sup>, E. I. Novikova<sup>2</sup>, G. De Geronimo<sup>4</sup>, M. G. Baring<sup>5</sup>, A. K. Harding<sup>6</sup>, J. Grindlay<sup>7</sup>, J. S. Hong<sup>7</sup>

(1) Washington University in St. Louis and McDonnell Center for the Space Sciences, St. Louis, MO, (2) High-Energy Space Environment Branch, Naval Research Laboratory, Washington, DC, USA, (3) Praxis, Inc., Alexandria, VA, USA, (4) Instrumentation Division, Brookhaven National Laboratory, Upton, NY, USA, (5) Department of Physics & Astronomy, Rice University, Houston, TX, USA, (6) Astrophysics Science Division, NASA Goddard Space Flight Center, Greenbelt, MD, USA, (7) Harvard-Smithsonian Center for Astrophysics, Cambridge, MA, USA.

**Abstract**—We report on the design and estimated performance of a balloon-borne hard X-ray polarimeter called HX-POL. The experiment uses a combination of Si and Cadmium Zinc Telluride detectors to measure the polarization of 50 keV–400 keV X-rays from cosmic sources through the dependence of the angular distribution of Compton scattered photons on the polarization direction. On a one-day balloon flight, HX-POL would allow us to measure the polarization of bright Crab-like sources for polarization degrees well below 10%. On a longer (15–30 day) flight from Australia or Antarctica, HX-POL would be able to measure the polarization of bright galactic X-ray sources down to polarization degrees of a few percent. Hard X-ray polarization measurements provide unique venues for the study of particle acceleration processes by compact objects and relativistic outflows. In this paper, we discuss the overall instrument design and performance. Furthermore, we present results from laboratory tests of the Si and CZT detectors.

## I. INTRODUCTION

X-RAY astronomy has made major contributions to modern astronomy and cosmology for the last three to four decades. To name a few examples, X-rays allowed us to study the hot gas in which the galaxies of galaxy clusters are embedded, to study gas briefly before it plunges into stellar mass and supermassive black holes, and to study mass accreting neutron stars. Presently, the National Aeronautics and Space Administration (NASA) and the European Space Agency (ESA) fly the Chandra and XMM-Newton soft X-ray telescopes, which set world records in terms of angular resolution (Chandra: 0.5") and collection area (XMM-Newton: 4,300 cm<sup>2</sup> at 1.5 keV). Even though X-ray astronomy has been extremely successful over several decades, there are still largely unexplored areas which future space-borne X-ray telescopes can pioneer. The NuSTAR hard X-ray telescope<sup>1</sup> is scheduled for launch in 2011 and will image 6–80 keV X-rays with an angular resolution of 40". The International X-ray Observatory (IXO)<sup>2</sup> would enable high-throughput excellent energy resolution ( $E/\Delta E > 2400$  at 6 keV) X-ray spectroscopy in the 0.3–10 keV energy band. The EXIST black hole finder

probe<sup>3</sup> would use coded mask imaging to scrutinize the entire sky every 170 min in the 5 keV to 600 keV energy band.

This paper focuses on X-ray polarimetry, another very promising and largely unexplored area. X-ray polarimetry would increase the parameter space for the study of compact objects like black holes and neutron stars from two dimensions (time variability and energy spectra) to four dimensions, by adding two qualitatively new parameters: polarization degree and polarization direction [1], [2], [3], [4]. The polarization measurements can be used to identify the processes responsible for the observed X-ray emission, to constrain viewing perspectives and opacities in accretion disk systems, and to gain access to the properties of the magnetic field (order and orientation) in the emission regions. Recently, concepts have been developed to measure the polarization of soft X-rays by tracking the photo-effect electrons that tend to be ejected parallel to the electric field vector of the X-rays with gas pixel detectors [5] and with time projection chambers [6]. At >20 keV energies, the Compton effect can be used to measure the polarization, as photons are preferentially scattered in the direction perpendicular to the electric field vector. Early soft X-ray polarization measurements were done with the OSO 8 experiment which used mosaic crystals of graphite to yield polarization-sensitive Bragg reflection of 2.6 keV and 5.2 keV X-rays [7]. The Ge detectors on board the INTEGRAL  $\gamma$ -ray observatory were used to measure the polarization of gamma-rays based on Compton effect polarimetry [8]. Recently, NASA approved the Gravity and Extreme Magnetism SMEX (GEMS) mission as a "small explorer mission". GEMS will combine grazing incident X-ray mirrors with time projection chamber detectors to measure the polarization of 2–10 keV X-rays, and will be launched in the next decade [9]. The Japanese ASTRO-H mission (formerly called "NeXT") will have a "soft  $\gamma$ -ray telescope" which uses Si and CdTe detector stacks and will have polarization sensitivity in the  $\gamma$ -ray energy regime [10].

The OSO 8 observations revealed a polarization degree of  $\sim 20\%$  of the 2.6 keV and 5.2 keV X-ray emission from the Crab Nebula, and a polarization angle aligned around

<sup>1</sup><http://www.nustar.caltech.edu/>

<sup>2</sup><http://ixo.gsfc.nasa.gov/>

<sup>3</sup><http://exist.gsfc.nasa.gov/>

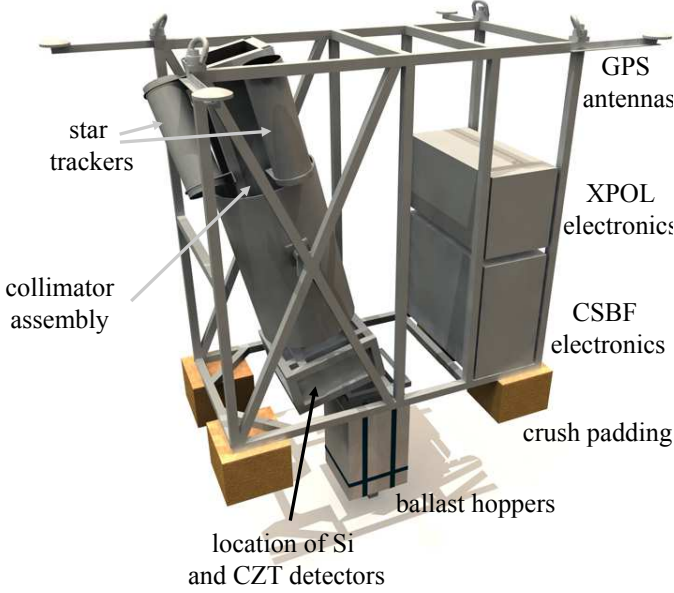


Fig. 1. Conceptual design of the HX-POL balloon payload. The polarization is measured with a Si-CZT detector configuration inside a 2 m high collimator-shield assembly. The collimator is pointed towards a source by rotating the gondola and by changing the elevation.

30 degrees oblique to the X-ray jet [7]. In the 0.1-1 MeV energy range, the INTEGRAL observations showed a high polarization degree of  $46\% \pm 10\%$ , and a polarization direction aligned with the orientation of the X-ray jet [8]. The result indicates that the X-ray emission comes from the inner jet. The fact that the polarization angle differs from the classic X-ray band to the soft gamma-ray band provides a significant diagnostic on the jet-nebula environment. It may be a general trend that polarization fractions increase with the energy of the X-rays, as the electrons emitting higher-energy X-rays lose their energy faster than the electrons responsible for the lower-energy X-rays; as a consequence, the regions responsible for harder X-rays should be more compact and thus more uniform than the regions responsible for soft X-rays. A more uniform magnetic field would lead to a higher degree of polarization. However, such trends would critically depend on the relative order of the magnetic field on different spatial scales, a salient property for MHD and plasma models. Even at balloon altitudes of  $\sim 40$  km, the atmosphere is only transparent for  $>20$  keV X-rays. Soft X-ray polarimeters have thus to be space borne. In the hard X-ray energy band, balloon-borne experiments with  $\sim 500$  cm<sup>2</sup> detection areas can measure polarization fractions of between 10% and a few percent for bright, mostly galactic sources with fluxes between 10% and 100% of the flux from the Crab Nebula. The measurement of the hard X-ray polarization of very short transient events (Gamma Ray Bursts, GRBs) and most extragalactic sources requires larger, most likely, space-borne experiments.

In Sect. II, the concept of the hard X-ray polarimeter HX-POL is presented, a balloon-borne experiment that uses Si and Cadmium Zinc Telluride (CZT) detectors. In Sect. III, the

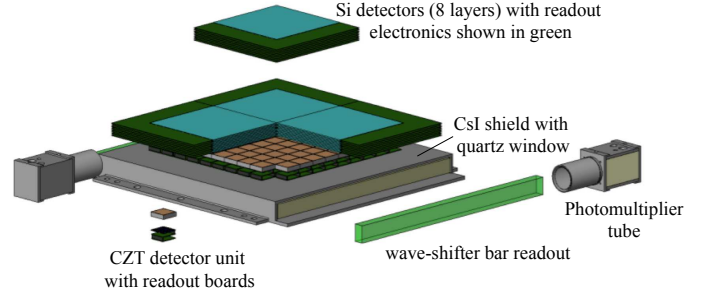


Fig. 2. “Exploded view” of the HX-POL detector assembly. A total of 32 Si detectors (each  $0.2 \text{ cm} \times 10 \text{ cm} \times 10 \text{ cm}$ , active detector area:  $81 \text{ cm}^2$ ) are tiled and stacked to make a 1.6 cm thick detector module with an active detection area of  $324 \text{ cm}^2$ . The Si detectors are positioned “above” one hundred CZT detectors (each  $0.5 \text{ cm} \times 2 \text{ cm} \times 2 \text{ cm}$ ) with an active detection area of  $400 \text{ cm}^2$ . The ASIC readout of the Si detectors is located at the perimeter of the Si detectors and the readout of the CZT detectors is located below the CZT detectors. The Si-CZT detectors are positioned above a  $2 \text{ cm} \times 25 \text{ cm} \times 25 \text{ cm}$  CsI active rear shield.

science potential is discussed, and in Sect. IV the results are summarized.

## II. DESCRIPTION OF THE HX-POL EXPERIMENT

### A. Overall design, minimization of systematic errors, calibration

HX-POL is a concept of a balloon-borne X-ray polarimeter that can measure the polarization of bright X-ray sources in the 50-400 keV energy range. Sketches of the gondola and the main detector assembly are shown in Figs. 1 and 2, respectively. The main detector assembly is made of Si and CZT detectors with an active detector area of  $324 \text{ cm}^2$  (Fig. 2). Photons Compton scatter in the low-Z Si and are photo-absorbed in the high-Z CZT detectors. The polarization can be inferred by analyzing the distribution of the azimuthal scattering angles. In addition to giving a high fraction of “golden events” with exactly one interaction in a Si detector and one in a CZT detector, the high-Z/low-Z detector combination avoids the background of neutron events which can mimic Compton scattered photons.

The Si detector assembly is made of 8 layers of 2 mm thick cross-strip Si detectors (strip pitch: 1.4 mm), giving a total thickness of 1.6 cm. Each of the 8 layers is made of an array of four  $0.2 \text{ cm} \times 10 \text{ cm} \times 10 \text{ cm}$  Si detectors (geometric area:  $100 \text{ cm}^2$ , active detector area:  $81 \text{ cm}^2$ ). The Si detector assembly is located above an array of  $10 \times 10$  CZT detectors. Each CZT detector has a volume of  $0.5 \text{ cm} \times 2 \text{ cm} \times 2 \text{ cm}$  and is contacted

with 64 pixels (pixel pitch: 2.5 mm). The data acquisition is triggered by a  $>20$  keV hit in one of the CZT detectors with or without a coincident hit in the Si detectors. A coincidence unit flags Si and CZT events if the two components triggered within a coincidence window of 2 micro-seconds. HX-POL's energy resolution includes contributions of the Si and CZT detectors and will be about 6% in the 100 keV-150 keV energy region where the instrument sees most events.

The detector assembly resides in a 2 m high collimator assembly that shields the detectors and limits their field of view to a  $\sim 8.4^\circ \times 8.4^\circ$  region of the sky. Sources are observed by alternating between observations of the source (ON-observations), and observations of a nearby background region (OFF-observations) to enable proper background subtraction. The collimator has a cross section that is larger than the cross section of the detector system, resulting in a “flat” angular response and in relaxed pointing requirements. The graded collimator-shield is made of 4 mm lead. Thin tin and copper layers at the inside of the collimator absorb fluorescent X-ray emission from the lead layer. The Si and CZT detectors reside above an active shield (CsI(Na),  $2\text{ cm} \times 25\text{ cm} \times 25\text{ cm}$ ) that reduces the atmospheric and internal backgrounds (e.g. events initiated by neutron capture in the CZT detectors) [11].

Polarization measurements are notorious for systematic effects that may mimic a polarization signal. The HX-POL design copes with systematic errors by rotating the entire collimator-detector assembly around the azimuthal axis at a frequency of about 0.05 Hz. After every  $360^\circ$  rotation the sense of rotation is reversed. The rest of the balloon payload does not participate in the rotation. The collimator-detector assembly has a mass of 150 kg, and the minimization of torques that adversely affect the pointing of the collimator are an important design consideration. The azimuthal distribution of Compton scattered events can then be analyzed in celestial coordinates (to extract the polarization of the emission) and in detector coordinates (to estimate systematic errors). Analysis of the ON/OFF data can be used to study effects related to the orientation of the X-ray collimator relative to the vertical axis, and relative to the geomagnetic field. The RHESSI experiment was rotated at 0.25 Hz, a property that was exploited for polarimetry measurements [12], [13]. The laboratory calibration would include tests with polarized and un-polarized beams of gamma-rays located at different positions relative to the collimator-detector assembly. We have started first tests of a Si+CZT prototype experiment with polarized and un-polarized gamma-rays at Washington University. Both tests use a 5 mCi  $^{137}\text{Cs}$  source. A tagged beam of polarized gamma-rays is produced by scattering the gamma-rays off a scintillator with photomultiplier readout.

### B. Si detector assembly

We chose Silicon Cross Strip Detectors (SCSDs) as the low-Z component of HX-POL. Si has a low atomic number of 14 which makes it a good Compton scatterer, and Si detectors have excellent energy and spatial resolution, even at room temperature. When cooled to temperatures of between  $-40^\circ\text{C}$  and  $-20^\circ\text{C}$ , they achieve energy resolutions close to those of

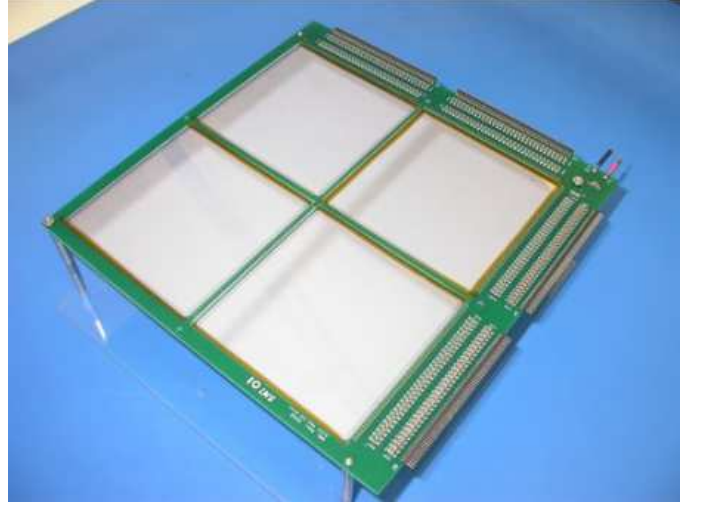


Fig. 3. Photo of a  $2 \times 2$  array of 2 mm thick silicon strip detectors, each with a geometric area  $100\text{ cm}^2$  and an active area of  $81\text{ cm}^2$ . On the top side and on the right side, the resistors and capacitors for AC-coupling the crossed strips on the two sides of the detectors can be seen.

Ge detectors. An interacting gamma ray deposits energy in the SCSD which leads to charge induced in the electrodes above and below the interaction. The amount of charge collected is directly proportional to the energy deposited in the detector. The strips on each side of the detector are perpendicular to each other (see the biasing components on two sides of the detector in Fig. 3). The interaction location is defined as the overlapping region where strips from each electrode collected the charge [14].

HX-POL uses 2 mm thick Si detectors with an area of  $10 \times 10\text{ cm}^2$  contacted with crossed anode and cathode strips with a strip pitch of 1.4 mm. The strips on each side of the detector are surrounded by a guard ring structure. The active area of each Si detector is  $81\text{ cm}^2$ . The eight layers of 2 mm thick Si detectors absorb vertically incident 50-100 keV X-rays with a probability of  $\sim 50\%$ . Figure 3 shows an array of four 2 mm thick Si detectors. The packaging of the Si-detectors in trays with eight layers of Si detectors is still under development.

Both the Si and the CZT detectors are read out with the NCI-ASIC developed by the Brookhaven National Laboratory and the NRL [15], [16]. The ASIC combines excellent noise performance with a sufficiently large dynamic range ( $>100$ ) and low power dissipation (5 mW/channel). For each of its 32 channels, the ASIC provides a low-noise preamplifier [17], [18], a fifth order filter (shaper) with baseline stabilizer [19], a threshold comparator, and a peak detector with analog memory [20]. The ASIC properly processes charges of either polarity by using a design with low-noise continuous reset circuits for each polarity [18], [21], [22]. Presently, the ASIC is used over the dynamic range from 12 keV to 2.8 MeV. Minor design changes should lead to a lower ASIC threshold of between 2.5 keV and 5 keV. The noise performance measured with the ASIC is shown in the upper panel of Fig. 4. For the detector capacitances relevant to HX-POL, the ASIC gives an ambient temperature dependent readout noise of between 1 keV and 2

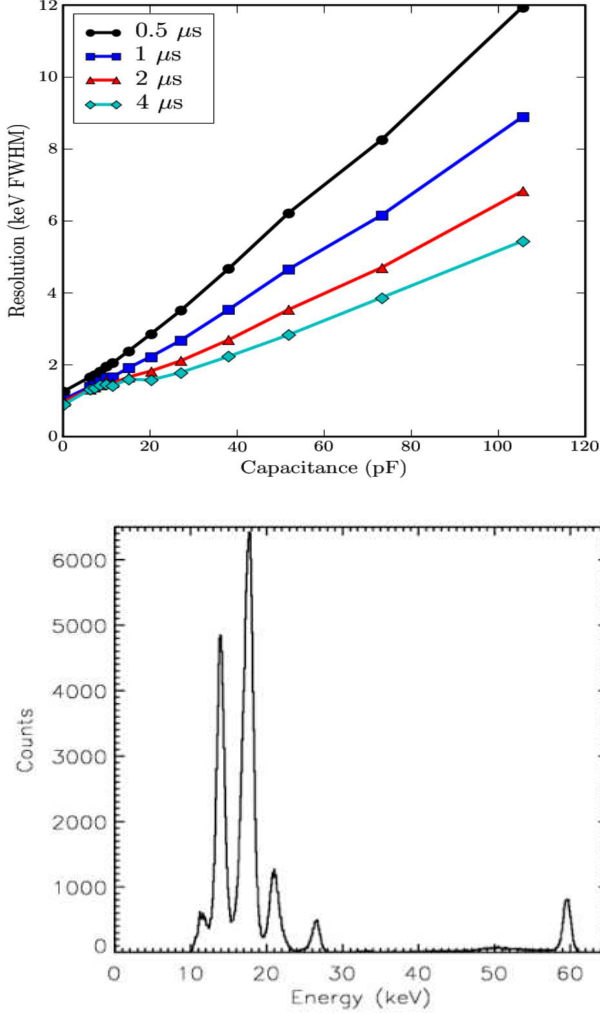


Fig. 4. The upper panel shows the measured room temperature resolution of the NCI-ASIC as a function of the input capacitance and shaping time. The resolutions refer here to Si. The lower panel shows an  $^{241}\text{Am}$  energy spectrum obtained with one 2 mm thick, 10 cm  $\times$  10 cm Si detector, identical to the detectors that will be used for HX-POL. The detector was cooled to  $-40^\circ\text{C}$  for this measurement. The 59.5 keV FWHM resolution is 2 keV.

keV.

The 2 mm thick Si detectors achieve excellent energy resolution. The energy resolution of one of the HX-POL Si detectors is shown in Fig. 4. At 59.5 keV the energy resolution is 2 keV. The detector was cooled to  $-40^\circ\text{C}$  for this measurement.

### C. CZT detector assembly

CZT is the detector material of choice for the high-Z component of HX-POL. CZT has a high average atomic number of  $\sim 50$  and thus has high stopping power and a high cross section for photo-effect interactions. At 100 keV, a 0.5 cm thick CZT detector absorbs  $\sim 99\%$  of incoming 100 keV X-rays, and  $\sim 90\%$  of the first interactions are photo-effect interactions. Other important characteristics are operation at room temperature, mm-spatial resolution, and good energy resolution. HX-POL will use 0.5 cm thick,  $2 \times 2\text{ cm}^2$  area

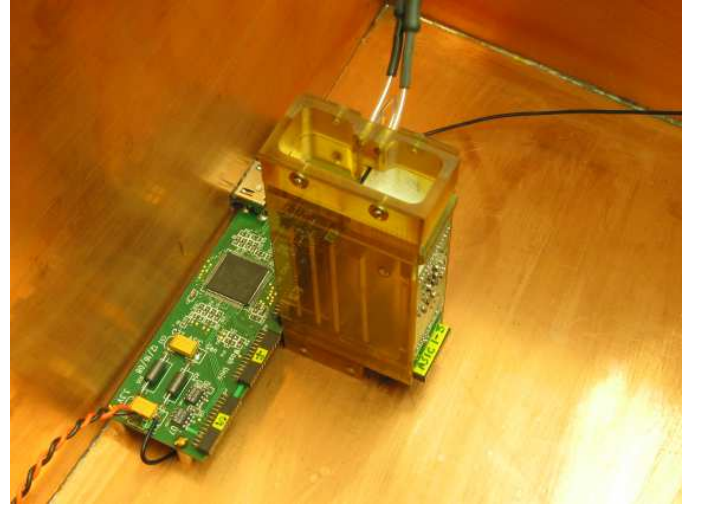


Fig. 5. Readout electronics for the CZT array. The photograph shows two CZT detectors (each:  $0.5 \times 2 \times 2\text{ cm}^2$ , 64 pixels) mounted in a plastic holder. The pixels are at the sides of the detectors facing the readout electronics. Inside the plastic holder reside five boards that hold five ASICs. Four ASICs are used to read out the pixels of the two detectors, and one ASIC is used to read out the cathodes. Several pairs of detectors can be daisy chained to form a “detector chain”. The “harvester board” (visible on the left side) can read out up to five detector chains.

CZT detectors contacted with 64 pixels at a pitch of 2.5 mm. Our previous results obtained with such detectors are described in [23], [24] and references therein. In the 50 keV–100 keV energy range, photons lose only a small fraction of their energy in Compton interactions, and the low-energy threshold of the HX-POL experiment is determined by the low-energy threshold of the Si detectors and not by the low-energy threshold of the CZT detectors.

The CZT detectors are read out with the same ASICs used for the Si detectors. Fig. 5 shows the present version of the readout system. The readout is designed to read multiple CZT detectors arranged in close proximity to form a “mosaic” of CZT detectors. The CZT detectors are lined up in rows and columns. Currently, the readout system can handle 5 rows with 5 CZT’s per row, allowing for a mosaic of 25 detectors. This can easily be expanded for larger mosaics in the future. Each row is made up of “pair modules” daisy chained together. A pair-module has 2 CZT detectors (64 pixels each) mounted on a “detector board”. Directly under the detector board, placed vertically, are five “ASIC boards”. Four ASIC boards (each with 32 channels) read the anode pixels and a fifth ASIC board reads the cathode signals. The ASIC boards contain the ASICs plus 12-bit A/D converters and voltage regulators. They plug into a motherboard, placed horizontally, which passes digital signals from the ASIC boards to the “digital readout board” directly below it. The digital readout board contains one Field Programmable Gate Array that reads out the five ASICs and transmits data in a serial data stream. This configuration of boards, making up one pair module, fits below the footprint of the two CZT detectors, allowing for pairs of detectors to be placed side-by-side. Serial data from the digital readout board is daisy chained to a “harvester board”. The harvester board reads out all five rows of pair modules

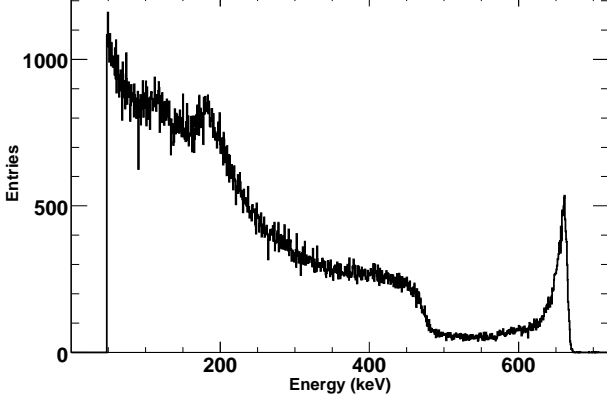


Fig. 6. Energy spectrum taken with an 0.5 cm thick CZT detector. The detector was operated at an energy threshold of 50 keV. The 662 keV energy resolution of the particular pixel shown here is 1.8% FWHM.

and transmits the data serially to the CPU. Data transfers are serial LVDS (Low Voltage Differential Signaling), transmitting at a rate of 3.125 Mbits/sec. Dead time for an event is 125 microseconds, although we expect that this can be reduced to 70 microseconds.

Fig. 6 shows a  $^{137}\text{Cs}$  energy spectrum taken with an 0.5 cm thick CZT detector and a prototype version of the ASIC-readout. The detector was operated at an energy threshold of 50 keV. The particular channel achieves an 662 keV energy resolution of 1.8% FWHM. Note that the design of the CZT detector array is still evolving. Right now, the detectors are mounted in plastic holders and make contact through spring loaded pogo pins. An HX-POL flight module would use CZT detectors permanently mounted to ceramic chip carriers. We are furthermore working on reducing the size of the readout electronics.

### III. SCIENTIFIC OBJECTIVES

We studied the performance of the HX-POL experiment with the GEANT 4 package [25] including the low-energy electromagnetic processes package GLECS [26]. The simulations assume a Crab spectrum [27] and a balloon flight at a (zenith-angle averaged) atmospheric depth of  $3 \text{ gr cm}^{-2}$ . For this depth, the transmissivity of the residual atmosphere increases rapidly from 0 to 0.6 in the 20 keV to 60 keV energy range and increases slowly at higher energies. The code simulates the energy resolution of the Si and CZT detectors and the discretization of the location information introduced by the strip pitch of the Si detectors and the pixel pitch of the CZT detectors. Two data samples were simulated: one with a polarization signature (the “ON-data sample”) and one without (the “OFF data sample”). The analysis of the simulated data uses only information that will also be available experimentally: the signal amplitudes measured in the Si strips and in the CZT pixels. If more than two interactions are recorded (taking into account the spatial resolution of the detectors), only the two highest energy deposits are used to determine the azimuthal scattering angle.

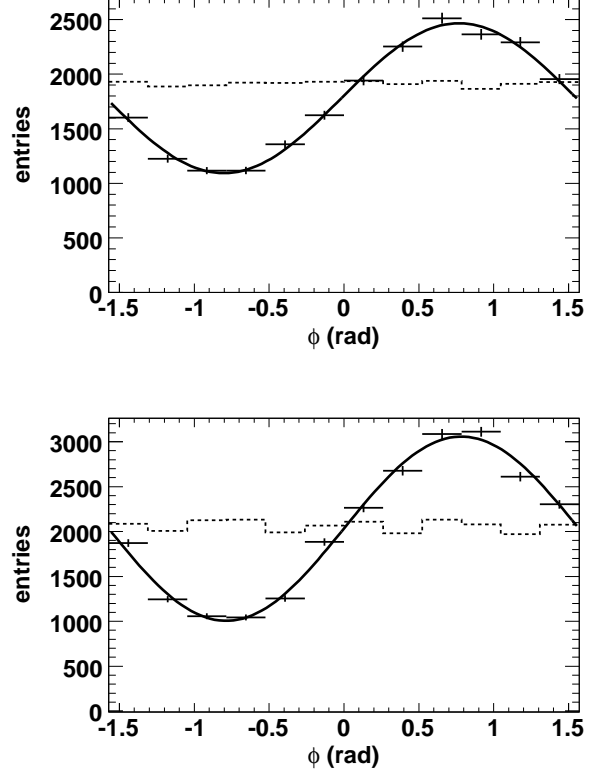


Fig. 7. Results from the HX-POL simulations. The panels show the distributions of azimuthal scattering angles for events with a  $>5 \text{ keV}$  Si detector hit and a  $>50 \text{ keV}$  CZT detector hit (upper panel), and for photons with a  $>5 \text{ keV}$  hit in at least two Si detectors (lower panel) for 100% polarized X-ray beams (solid lines) and an un-polarized beams (dashed lines). A source with the flux from the Crab Nebula was assumed and an ON-observation time of 3 hrs. The absolute numbers of counts correspond to 3 hour observations of an X-ray source with the flux and spectrum of that of the Crab Nebula.

Figures 7 and 8 show results for 100% polarized and un-polarized X-ray beams (no backgrounds). The absolute number of events correspond to a 3 hr ON-observation of a source with the flux and spectrum of that of the Crab Nebula [27] (the emission from the Crab Nebula is of course not polarized to 100%). The upper panel of Fig. 7 shows the distribution of azimuthal scattering angles for “Si-CZT” events where one Si detector records a hit (most likely from a Compton interaction) and one CZT detector pixel records a hit (most likely from a photo-effect interaction). The lower panel of Fig. 7 shows the same for “Si-Si” events with hits in two or more Si detectors. The analysis of Si-Si events discards events in which the two highest energy depositions are less than 3.2 pixel pitches away from each other when projected onto the plane of the detectors. This cut leads to a rather even distribution of detected azimuthal scattering angles. The events that do not pass this cut also hold information and could be used in a more sophisticated analysis.

The modulation factor is defined as

$$\mu = \frac{C_{\max} - C_{\min}}{C_{\max} + C_{\min}} \quad (1)$$

where  $C_{\max}$  and  $C_{\min}$  refer to the maximum and minimum

TABLE I  
HX-POL MINIMUM DETECTABLE POLARIZATION (MDP).

Events	$\mu$	$R_{\text{src}}$ [Hz]	$R_{\text{bg}}$ [Hz]	MDP [%]
Si-CZT	0.40	2.0	0.13	7.7
Si-Si	0.50	2.3	0.14	5.8
All	0.46	4.3	0.27	4.7

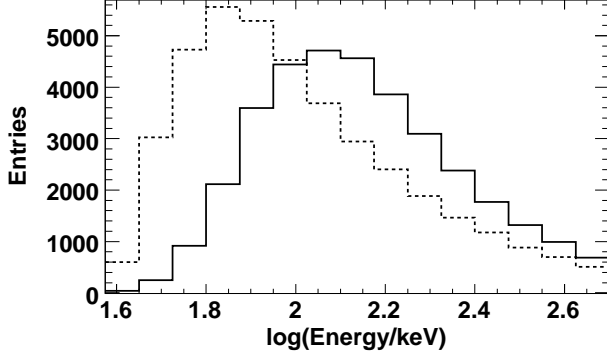


Fig. 8. The panel shows the energy distribution of photons producing Si-CZT events (solid line) and Si-Si events (dashed line).

counts detected for different azimuthal scattering angles. For the Si-CZT and the Si-Si events the modulation factors are  $\mu_{\text{Si-CZT}} = 0.4$ , and  $\mu_{\text{Si-Si}} = 0.5$ , respectively. The simulations can be used to determine the minimum detectable polarizations (MDP). We compute the 99% confidence level MDP with a modified version of the Equation (10) in [28] that accounts for the statistical errors of the OFF-data:

$$\text{MDP} = \frac{4.29}{\mu R_{\text{src}}} \sqrt{\frac{R_{\text{src}} + 2 R_{\text{bg}}}{T}} \quad (2)$$

where  $R_{\text{src}}$  is the total source counting rate,  $R_{\text{bg}}$  is the total background counting rate and  $T$  is the ON integration time (assumed to equal the OFF integration time).

Table I lists the values  $R_{\text{src}}$ ,  $R_{\text{bg}}$ , and MDP for the Si-CZT events, the Si-Si events, and for both types of events. We assume interspersed ON-OFF observations with a ON and OFF integration time of 3 hrs each. The background was adopted from the balloon results reported by Schönfelder et al. [29]. The prediction of the sensitivity of the Si-CZT events should be robust. The sensitivity of the Si-Si events will be poorer than stated in Table I, as we did not attempt to model neutrons. Elastically scattering neutrons can mimic Compton-events. Figure 8 shows the distribution of the energy of the Si-CZT events and the Si-Si events. Most Si-CZT events have energies between 60 keV to 400 keV. Most Si-Si events have energies between 50 keV and 300 keV.

Figure 9 shows the measured polarization degree for simulated observations of the Crab Nebula. For this graph, only Si-CZT events were used. For a balloon launch from Fort Sumner (NM) or Palestine (TX), the Crab Nebula can be observed for 6 hours at zenith angles smaller than  $40^\circ$ . We thus assumed an observation with 3 hours of ON-time and 3 hours of OFF-time. As before, we use a zenith angle averaged residual atmosphere

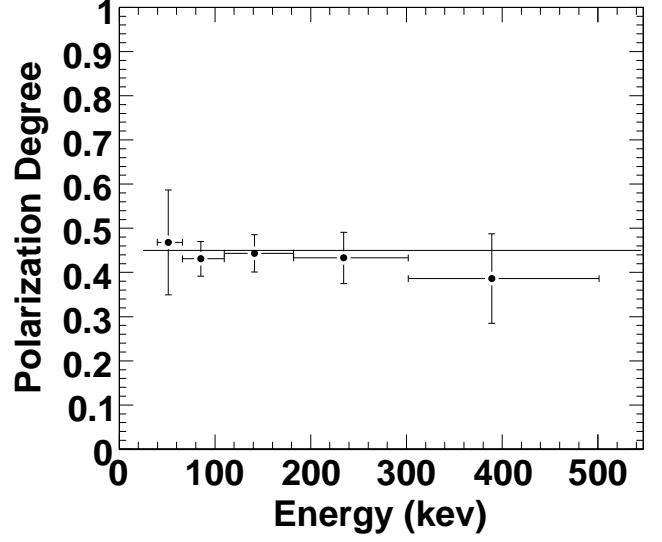


Fig. 9. The graph shows the results of a simulated observation of the Crab Nebula (3 hours ON, 3 hours OFF). The polarization degree can be measured in several independent energy bins.

of  $3 \text{ gr cm}^{-2}$ . The graph shows that HX-POL will be able to measure the polarization of the Crab Nebula in several independent energy bins.

Additional observation targets for a one-day balloon-flight are black hole binaries and accreting neutron stars. The binary black holes Cygnus X-1 and GRS 1915+105 are prime targets because of their X-ray brightness. Cygnus X-1 is an exceptional source as it shows persistent flaring activity. In the HEAO-4 survey it was the brightest  $> 80 \text{ keV}$  source [30]. The source GRS 1915+105 is well known for frequent flaring epochs with a stunning diversity of flux and spectral patterns [31]. Binary black holes exhibit different emission states (thermal, hard, and steep power law) that depend on the structure of the accretion disk and the accretion disk corona, and on the relative importance of a relativistic outflow (jet) [32]. Synchrotron emission and Compton scatterings could both lead to polarization degrees that are observable with HX-POL. Bright accreting neutron stars are Hercules X-1 and Cen X-3. Owing to the emission mechanism and to the propagation of the X-rays through the highly magnetized plasma surrounding the neutron stars, the X-rays from these objects might exhibit polarization degrees of several 10% (e.g. [33], [4]).

On a longer 15-30 day long balloon flight, HX-POL would be able to scrutinize the polarization in strong galactic sources to a level of a few percent. Deep observations could be used to measure the energy dependence of the polarization of the X-ray emission from binary black holes. These measurements would constrain the dominant emission process as a function of energy. In high magnetic-field pulsars and magnetars, photon splitting (a higher order QED effect) could produce strong energy-dependent polarization leading up to a high-

energy cut-off [34], [35]. This effect cannot be observed in terrestrial laboratories and would provide a powerful test of QED in extreme conditions.

A longer balloon flight would have a realistic chance to measure the polarization of the hard X-rays from extragalactic sources, e.g. from “extreme synchrotron blazars”, mass-accreting supermassive black holes with highly relativistic jets pointing at the observer [36]. Their synchrotron emission extends into the very hard X-ray regime. For example, for Mrk 501, the BeppoSAX mission measured a spectral energy distribution with a “low-energy” component peaking in the  $>100$  keV energy range [37]. The high-energy component, presumably inverse Compton emission, peaks in the GeV/TeV energy range [38]. Extreme synchrotron blazars show long lasting periods (3 months or more) of intense flaring activity. A positive detection of a high polarization degree would show that the magnetic fields in AGN jets are well ordered in the “blazar zone”  $\sim 1$  pc away from the black hole, and would add an important constraint to models of jet formation.

#### IV. SUMMARY AND CONCLUSIONS

This paper describes the concept of a balloon-borne hard X-ray polarimeter. The detector module combines a low-Z Compton scatterer (Si) with a high-Z photoeffect absorber (CZT). The detector combination achieves excellent polarization sensitivity in the 50 keV to 400 keV energy band. Based on 3+3 hrs of ON-OFF observations during a one-day balloon flight, the polarization of strong Crab-like sources can be measured for polarization degrees well below 10%. On a 15-30 day balloon flight, polarization degrees of a few percent can be measured. The 50-400 keV energy band is well suited for a balloon-borne experiment: atmospheric absorption hinders observations below 20 keV and observations above 400 keV have to deal with very low photon fluxes and require relatively large experiments and/or long integration times, both better suited for space borne experiments. One of the strengths of the Si/CZT detector combination is the excellent energy resolution that makes it possible to measure the energy dependence of the polarization properties. Compared to experiments that use Si detectors only, the Si/CZT combination avoids the neutron backgrounds that plague experiments exclusively made of low-Z detectors. Compared to experiments that use CZT only, the Si/CZT combination achieves a lower energy threshold. In CZT detectors, photoeffect interactions dominate over Compton interactions up to energies of  $\sim 250$  keV; furthermore,  $<100$  keV photons are absorbed quickly in CZT, making it necessary to use CZT detectors with very small pixel pitches.

#### ACKNOWLEDGMENT

The Washington University group acknowledges support by NASA (grant NNX07AH37G).

#### REFERENCES

- [1] Rees, M. J., “Expected polarization properties of binary X-ray sources”, *MNRAS*, vol. 171, pp. 457-465, June 1975.
- [2] Lightman, A. P., Shapiro, S. L., “Spectrum and polarization of X-rays from accretion disks around black holes”, *ApJ*, vol. 198, pp. L73-L75, June 1975.
- [3] Lightman, A. P., Shapiro, S. L., “Polarization of X-rays from Cygnus X-1 - A test of the accretion disk model”, *ApJ*, vol. 203, pp. 701-703, Feb. 1976.
- [4] Meszaros, P., Novick, R., Chanan, G. A., Weisskopf, M. C., “Astrophysical implications and observational prospects of X-ray polarimetry”, *ApJ*, vol. 324, pp. 1056-1067, Jan. 1988.
- [5] Costa, E., Bellazzini, R., Bregeon, J., et al., “XPOL: a photoelectric polarimeter onboard XEUS”, *Proc. SPIE*, vol. 7011, pp. 15-19, arXiv0810.2700C.
- [6] Hill, J. E., Barthelmy, S., Black, J. K., et al., “A burst chasing x-ray polarimeter”, *SPIE*, vol. 6686, 29, pp. 66860Y-66860Y-12, Sept. 2007.
- [7] Weisskopf, M. C., Silver, E. H., Kestenbaum, H. L., Long, K. S., Novick, R., “A precision measurement of the X-ray polarization of the Crab Nebula without pulsar contamination”, *ApJL*, vol. 220, L117-L121, March 1978.
- [8] Dean, A. J., Clark, D. J., Stephen, J. B., et al., “Polarized Gamma-Ray Emission from the Crab”, *Science*, vol. 321, issue 5893, 1183-1185, Aug. 2008.
- [9] <http://heasarc.gsfc.nasa.gov/docs/gems/>
- [10] Takahashi, T., Kelley, R., Mitsuda, K., et al., “The NeXT Mission”, *Space Telescopes and Instrumentation 2008: Ultraviolet to Gamma Ray*. Edited by Turner, Martin J. L.; Flanagan, Kathryn A. Proceedings of the SPIE, Volume 7011, pp. 70110O-70110O-14, 2008.
- [11] Garson, III, A., Krawczynski, H., Grindlay, J., et al., “Using the active collimator and shield assembly of an EXIST-type mission as a gamma-ray burst spectrometer”, *A&A*, vol. 456, pp. 379-387, Sept. 2006.
- [12] McConnell, M. L., Ryan, J. M., Smith, D. M., Emslie, A. G., Fivian, M., Hurford, G. J., Lin, R. P., “RHESSI Studies of Solar Flare Hard X-Ray Polarization”, *Bulletin of the American Astronomical Society*, Vol. 36, p. 668, 2004.
- [13] Coburn, W., Boggs, S. E., “Polarization of the prompt  $\gamma$ -ray emission from the  $\gamma$ -ray burst of 6 December 2002”, *Nature*, vol. 423, pp. 415-417, 2003.
- [14] Kroeger, R. A., et al. 1995, In: “Hard X-ray and gamma-ray imaging systems utilizing germanium strip detectors”, eds. L. Bassani and G. di Cocco, Kluwer Press, 329.
- [15] Wulf, E. A., Philips, B. F., Johnson, N., Kurfess, J. D., Novikova, E. I., O’Connor, P., De Geronimo, G., “Compton imager for detection of special nuclear material”, *NIMA*, vol. 579, pp. 371-374, Aug. 2008.
- [16] de Geronimo, G., Fried, J., Frost, E., Philips, B. F., Vernon, E., Wulf, E. A., “Front-End ASIC for a Silicon Compton Telescope”, *IEEE Trans. Nucl. Sci.*, vol. 55, issue 4, pp. 2323-2328, Aug. 2008.
- [17] O’Connor, P., De Geronimo, G., “Prospects for charge sensitive amplifiers in scaled CMOS”, *NIMA*, vol. 480, issue 2-3, pp. 713-725, March 2002.
- [18] De Geronimo, G., O’Connor, P., Beuttenmuller, R. H., Li, Z., Kuczewski, A. J., Siddons, D. P., “Development of a high-rate high-resolution detector for exafs experiments”, *IEEE Trans. Nucl. Sci.*, vol. 50, issue 4, pp. 885-891, Aug. 2003.
- [19] De Geronimo, G., O’Connor, P., Grosholz, J., “A CMOS baseline holder (BLH) for readout ASICs”, *IEEE Trans. Nucl. Sci.*, vol. 47, pp. 818-822, June 2000.
- [20] De Geronimo, G., O’Connor, P., Kandasamy, A., “Analog CMOS peak detect and hold circuits. Part 2. The two-phase offset-free and derandomizing configuration”, *NIMA*, vol. 484, pp. 544-556, May 2000.
- [21] De Geronimo, G., O’Connor, P., “A CMOS fully compensated continuous reset system”, *IEEE Trans. Nucl. Sci.*, vol. 47, pp. 1458-1462, Aug. 2000.
- [22] De Geronimo, G., Fried, J., O’Connor, P., Radeka, V., Smith, G. C., Thorn, C., Yu, B., “Front-end ASIC for a GEM based time projection chamber”, *IEEE Trans. Nucl. Sci.*, vol. 51, issue 4, pp. 1312-1317, Aug. 2004.
- [23] Jung, I., Krawczynski, H., Burger, A., Guo, M., Groza, M., “Detailed studies of pixelated CZT detectors grown with the modified horizontal Bridgman method”, *Aph*, vol. 28, issue 4-5, pp. 397-408, Dec. 2007.
- [24] Li, Q., Garson, A., Jung, I., Groza, M., Dowkontt, P., Bose, R., Simburger, G., Burger, A., Krawczynski, H., “Test of CZT Detectors with Different Pixel Pitches and Thicknesses”, Conference record of NSS/MIC 2007 conference, October 2007, Hawaii [arXiv:0712.1178].
- [25] Agostinelli, S., et al. “GEANT4: A simulation toolkit”, *NIMA*, vol. 506, pp. 250-303, Jul. 2003.
- [26] Kippen, R. M., “The GEANT low energy Compton scattering (GLECS) package for use in simulating advanced Compton telescopes”, *New Astron. Rev.*, vol. 48, issue 1-4, pp. 221-225, Feb. 2004.
- [27] Tueller, J., Baumgartner, W. H., Markwardt, C. B., et al., “THE 22-MONTH Swift-BAT ALL-SKY HARD X-RAY SURVEY”, submitted to the *ApJS* (2009) [arXiv:0903.3037].

- [28] Weisskopf, M. C., Elsner, R. F., Hanna, D., Kaspi, V. M., O'Dell, S. L., Pavlov, G. G., Ramsey, B. D., "The prospects for X-ray polarimetry and its potential use for understanding neutron stars", Paper presented at the 363<sup>rd</sup> Heraeus Seminar in Bad Honnef, Germany, Springer Lecture Notes (in press), 2009, [arXiv:astro-ph/0611483]
- [29] Schoenfelder, V., Graser, U., Daugherty, J., "Diffuse cosmic and atmospheric MeV gamma radiation from balloon observations", *ApJ*, vol. 217, pp. 306-319, Oct. 1977.
- [30] Levine, A. M., Lang, F. L., Lewin, W. H. G., et al., "The HEAO 1 A-4 catalog of high-energy X-ray sources", *ApJS*, vol. 54, pp. 581-617, Apr. 1984.
- [31] McClintock, J. A., Remillard, R. 2006, In: "Compact Stellar X-Ray Sources", eds. W.H.G. Lewin and M. van der Klis, Cambridge University Press, Chapter 4.
- [32] Remillard, R. A., McClintock, J. E., "X-Ray Properties of Black-Hole Binaries", *ARA&A*, vol. 44, issue 1, pp. 49-92, Sept. 2006.
- [33] Kii, T., "X-ray polarizations from accreting strongly magnetized neutron stars - Case studies for the X-ray pulsars 4U 1626-67 and Hercules X-1", *Publ. Astron. Soc. Jap.*, vol. 39, no. 5, pp. 781-800, 1987.
- [34] Baring, M. G., Harding, A. K. "Photon Splitting and Pair Creation in Highly Magnetized Pulsars", *ApJ*, vol. 547, pp. 929-948, Feb. 2001.
- [35] Harding, A. K., Baring, M. G., Gonthier, P. L., "Photon-splitting Cascades in Gamma-Ray Pulsars and the Spectrum of PSR 1509-58", *ApJ*, vol. 476, pp. 246-260, Feb. 1997.
- [36] Costamante, L., Ghisellini, G., Giommi, P., et al., "Extreme synchrotron BL Lac objects. Stretching the blazar sequence", *A&A*, vol. 371, pp. 512-526, May 2001.
- [37] Pian, E., Vacanti, G., Tagliaferri, G., et al., "BeppoSAX Observations of Unprecedented Synchrotron Activity in the BL Lacertae Object Markarian 501", *ApJ*, vol. 492, L17-L21, Jan. 2001.
- [38] Krawczynski, H., Hughes, S. B., Horan, D., et al., "Multiwavelength Observations of Strong Flares from the TeV Blazar 1ES 1959+650", *ApJ*, vol. 601, issue 1, pp. 151-164, Jan. 2004.